COLD-MODE ACCRETION: DRIVING THE FUNDAMENTAL MASS–METALLICITY RELATION AT $z \sim 2$

GLENN G. KACPRZAK[1], FREEKE VAN DE VOORT[2,3], KARL GLAZEBROOK[1], KIM-VY H. TRAN[4], TIANTIAN YUAN[5],
THEMIYA NANAYAKKARA[1], REBECCA J. ALLEN[1,6], LEO ALCORN[4], MICHAEL COWLEY[6,7], IVO LABBÉ[8],
LEE SPITLER[6,7], CAROLINE STRAATMAN[8], AND ADAM TOMCZAK[9]

[1] Swinburne University of Technology, Victoria 3122, Australia; gkacprzak@astro.swin.edu.au
[2] Department of Astronomy and Theoretical Astrophysics Center, University of California, Berkeley, CA 94720-3411, USA
[3] Academia Sinica Institute of Astronomy and Astrophysics, P.O. Box 23-141, Taipei 10617, Taiwan
[4] George P. and Cynthia Woods Mitchell Institute for Fundamental Physics and Astronomy, and Department of Physics and Astronomy,
Texas A&M University, College Station, TX 77843-4242, USA
[5] Research School of Astronomy and Astrophysics, The Australian National University, Cotter Road, Weston Creek, ACT 2611, Australia
[6] Australian Astronomical Observatories, P.O. Box 915 North Ryde NSW 1670, Australia
[7] Department of Physics and Astronomy, Macquarie University, Sydney, NSW 2109, Australia
[8] Leiden Observatory, Leiden University, P.O. Box 9513, 2300 RA Leiden, The Netherlands
[9] Department of Physics, University of California Davis, One Shields Avenue, Davis, CA 95616, USA

ABSTRACT

We investigate the star formation rate (SFR) dependence on the stellar mass and gas-phase metallicity relation at $z = 2$ with MOSFIRE/Keck as part of the ZFIRE survey. We have identified 117 galaxies ($1.98 \leqslant z \leqslant 2.56$), with $8.9 \leqslant \log(M/M_{\odot}) \leqslant 11.0$, for which we can measure gas-phase metallicities. For the first time, we show a discernible difference between the mass–metallicity relation, using individual galaxies, when dividing the sample by low ($<10\,M_{\odot}\,\mathrm{yr}^{-1}$) and high ($>10\,M_{\odot}\,\mathrm{yr}^{-1}$) SFRs. At fixed mass, low star-forming galaxies tend to have higher metallicity than high star-forming galaxies. Using a few basic assumptions, we further show that the gas masses and metallicities required to produce the fundamental mass–metallicity relation and its intrinsic scatter are consistent with cold-mode accretion predictions obtained from the OWLS hydrodynamical simulations. Our results from both simulations and observations are suggestive that cold-mode accretion is responsible for the fundamental mass–metallicity relation at $z = 2$ and it demonstrates the direct relationship between cosmological accretion and the fundamental properties of galaxies.

Key words: cosmology: observations – galaxies: abundances – galaxies: evolution – galaxies: fundamental parameters – galaxies: high-redshift – intergalactic medium

1. INTRODUCTION

Mass and metallicity are arguably the most fundamental properties of galaxies, since they reflect stellar build-up/evolution and the cycling of baryons through outflows and accretion. A clear consequence of these processes is the galaxy stellar mass–metallicity relation, which has been observed up to $z \sim 4$ (e.g., Tremonti et al. 2004; Erb et al. 2006; Steidel et al. 2014; Troncoso et al. 2014; Zahid et al. 2014).

Cosmological simulations continue to show that cosmic accretion provides significant fuel for star formation, resulting in galaxy mass growth and chemical enrichment via outflows (Dekel et al. 2009; van de Voort & Schaye 2012). They also show that most of this gas accretes in the "cold-mode," i.e., without being heated by a virial shock (e.g., Kereš et al. 2005; Faucher-Giguère et al. 2011; van de Voort et al. 2011). Metal-poor cold-gas accretion has been observed on the periphery of galaxies, using absorption lines detected in background quasar spectra (e.g., Kacprzak et al. 2012; Bouché et al. 2013; Crighton et al. 2013), which are also dynamically consistent with large-scale cosmic web accretion (e.g., Steidel et al. 2002; Kacprzak et al. 2010). These inward flows are likely why, at a given stellar mass, metallicity is dependent on the star formation rate (SFR; Mannucci et al. 2010; Bothwell et al. 2013; Forbes et al. 2014; Maier et al. 2015).

It has been found that at a fixed mass, galaxies with high SFRs have lower gas-phase metallicities than galaxies with low SFRs. This fundamental mass–metallicity relation (FMR: see Mannucci et al. 2010) exhibits little scatter at $z = 0$, which implies an equilibrium between inflowing and outflowing gas and star formation. At higher redshifts, it is still questionable if a fundamental mass–metallicity relation exists because at $z \sim 2$, the mass–metallicity relation is highly scattered for stellar masses less than $10^{10}M_{\odot}$ (Sanders et al. 2015; Kacprzak et al. 2015; Tran et al. 2015). This observed scatter may not be surprising given that if a significant metal-poor accretion event occurs, which is especially common at high redshifts, it is expected that the galaxy's integrated metallicity decreases and that it experiences a boost in star formation. Thus, we should expect to see a fundamental mass–metallicity relation at higher redshifts as well.

The timescale between accretion and induced star formation is still uncertain. However, direct observations of metallicity and SFR profiles of local metal-poor galaxies have shown that highly star-forming regions within the galaxy have roughly a factor of 10 lower metallicity than the total galaxy metallicity, indicating that accreted gas is converted into stars within $\sim 100\,\mathrm{Myr}$ (Sánchez Almeida et al. 2015). Thus, this direct relation between accretion, SFR, and metallicity is critical for understanding galaxy formation and evolution.

We further explore the relationship between SFR and the mass–metallicity relation at $z \sim 2$, and examine the hypothesis that accretion could cause the scatter in the mass–metallicity relation. Here, we present Keck/MOSFIRE observations from the ZFIRE Survey (Nanayakkara et al. 2016) of 117 galaxies

for which we have gas-phase metallicities, stellar masses, SFRs, and gas masses described in Section 2. In Section 3, we show that there is a fundamental mass–metallicity relation driven by SFR. We further use our data, with some underlying basic assumptions, to compute the gas accretion masses and metallicities, which are shown to be in agreement with cosmological simulations. We adopt a $h = 0.70$, $\Omega_M = 0.3$, $\Omega_\Lambda = 0.7$ cosmology for our ZFIRE Survey.

2. MOSFIRE SPECTROSCOPIC OBSERVATIONS AND SAMPLE

The ZFIRE survey used Keck/MOSFIRE to spectroscopically identify 181 galaxies to date in the COSMOS field ($1.98 \leqslant z \leqslant 3.26$). The survey includes a Virgo-like progenitor at $z = 2.095$ (57 confirmed members) with a velocity dispersion of 550 km s^{-1} (Yuan et al. 2014). The spectroscopic targets were selected using the photometric redshifts from the K-band selected catalog from ZFOURGE (Straatman et al. 2016), which have an accuracy of $\Delta z/(1 + z_{\rm spec}) = 2\%$ (Yuan et al. 2014; Nanayakkara et al. 2016).

The MOSFIRE near-infrared K-band spectroscopic observations, data reduction, and flux calibration procedures are described in our ZFIRE Catalog (Nanayakkara et al. 2016). All spectra are converted to vacuum wavelengths. Our typical 3σ spectral flux limit is 1.8×10^{-18} erg s^{-1} cm^{-2}.

Gaussian profiles were simultaneously fit to Hα and [N II] emission lines, using both tied line centers and velocity widths, to determine their total flux. See Yuan et al. (2014) and Kacprzak et al. (2015) for some example 1D and 2D spectra. All spectra are flux-calibrated to their total K-band magnitudes to $<10\%$ (see Nanayakkara et al. 2016). We compute gas-phase oxygen abundances using the N2 relation of Pettini & Pagel (2004) where $12 + \log({\rm O/H}) = 8.90 + 0.57 \times {\rm N2}$ (N2 $\equiv \log([{\rm N\,II}]/{\rm H}\alpha)$). We require a 3σ detection significance level for [N II], otherwise 1σ detection limits are used.

Since Kacprzak et al. (2015) have shown that field and cluster galaxies exhibit identical mass–metallicity relations at $z = 2$ (<0.02 dex offset), we do not differentiate between galaxy environment in this work. This assumption is further validated by Kewley et al. (2016), showing that our $z \sim 2$ field and cluster galaxies have consistent ISM conditions. After removing AGNs (see Kacprzak et al. 2015; Cowley et al. 2016), our final sample consists of 117 galaxies ($1.98 \leqslant z \leqslant 2.56$, $\langle z \rangle = 2.160 \pm 0.008$) with 63 metallicity measurements and 54 metallicity limits. Our spectroscopic sample is mass complete down to $10^{9.3}\, M_\odot$ (see Nanayakkara et al. 2016).

We used stellar masses and stellar attenuation (A_V) computed from the photometry from ZFOURGE using Bruzual & Charlot (2003) stellar population models with FAST (Kriek et al. 2009), assuming solar metallicity, a Chabrier (2003) initial mass function, exponentially declining star formation histories, and constrained to the spectroscopic redshift (Straatman et al. 2016).

We derived attenuation corrected Hα SFRs using relations from Tran et al. (2015) for dust corrections and from Hao et al. (2011) to convert Hα fluxes to SFRs ($\log({\rm SFR}) = \log(L_{{\rm H}\alpha})$ -41.27). Attenuation corrections for both the stellar continuum correction (Calzetti et al. 2000) and nebular emission (Cardelli et al. 1989) are included (see Tran et al. 2015 for details).

3. RESULTS

3.1. Fundamental Mass–Metallicity Relation

In Figure 1 (left), we show the mass–metallicity relation at $z = 2$. We have metallicity measurements for a significant range of galaxy masses from $8.9 \leqslant \log(M/M_\odot) \leqslant 11.0$. As previously shown in Kacprzak et al. (2015) our fitted and stacked data are consistent with previous results from MOSDEF (Sanders et al. 2015), KBSS-MOSFIRE (Steidel et al. 2014) and Erb et al. (2006). We note that, consistent with previous works, there is a significant amount of scatter in metallicity for low-mass galaxies compared to what is observed at $z = 0$ (e.g., Tremonti et al. 2004).

The mass–metallicity relation in Figure 1 is shown as a function of low ($<10\, M_\odot$ yr^{-1}) and high ($>10\, M_\odot$ yr^{-1}) star-forming galaxies. Along with the data, we present a bootstrap fit (1000 times) using $12 + \log({\rm O/H}) = y_i + m_i(M_* - 10)$. We fit the data, which include the 1σ limits, using the expectation-maximization maximum-likelihood method of Wolynetz (1979). We find for galaxies with SFR $< 10\, M_\odot$ yr^{-1} a $y_{\rm SFR<10} = 8.46 \pm 0.03$ with a flat slope of $m_{\rm SFR<10} = 0.07 \pm 0.05$ and for galaxies with SFR $< 10\, M_\odot$ yr^{-1} a $y_{\rm SFR>10} = 8.37 \pm 0.01$ with a steeper slope of $m_{\rm SFR>10} = 0.42 \pm 0.03$. The fitted slopes of the low and high star-forming galaxies differ by 4.4σ.

We further stack the spectra with roughly an equal number of galaxies per bin. The spectra were stacked, weighting by the uncertainty spectrum, to determine the typical metallicity per mass bin as shown in Figure 1 (right). The stacked data are consistent with the fitted data. Both the individual metallicity measurements, stacked data, and fits suggest that there is a slope dependence of SFR on the mass–metallicity relation at the 4.4σ level whereby galaxies with lower SFRs have higher metallicity than galaxies with higher SFRs for a fixed mass at $M_* \lesssim 10^{10}\, M_\odot$.

We have further explored whether high and low star-forming galaxies, at fixed mass, have morphological differences. We find no discernible difference in their size and Sérsic index distribution between the two populations. A visual inspection of the morphologies and nearby companions of the two populations are also indistinguishable. Furthermore, both low and high star-forming galaxies have consistent distributions of stellar attenuation (A_V).

3.2. Total Gas Mass and Gas Accretion

Although we do not have direct measurements of galaxy gas masses, we compute galaxy total gas masses using the inverse Kennicutt–Schmidt Law, adopting the formalism from Papovich et al. (2015). Galaxy sizes are obtained from the catalog of van der Wel et al. (2012), which were measured from *Hubble Space Telescope*/WFC3 F160W ($\lambda_{\rm rest} = 4860$ Å) CANDELS multi-cycle treasury program (Grogin et al. 2011; Koekemoer et al. 2011). We obtain $108/117$ (92%) matches within a $0\farcs7$ aperture between our sample and the van der Wel et al. (2012) galaxy size catalog and present total gas masses for those 108 objects. In Figure 2, we show the total gas mass distribution, computed using the inverse Kennicutt–Schmidt Law, as a function of stellar mass for low and high star-forming galaxies.

Here we test the hypothesis that cosmic gas accretion, which is predicted to be significant at $z = 2$, drives the large scatter in the mass–metallicity relation and the SFR dependence. If we simply assume that galaxies having high SFRs are accreting
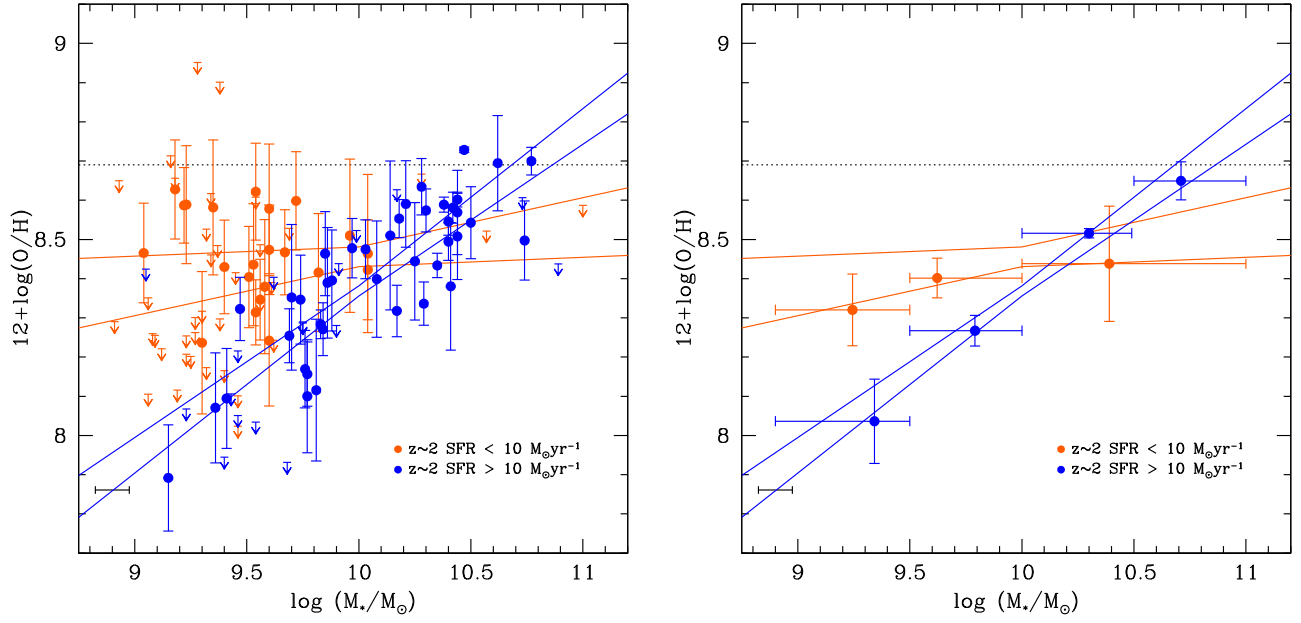
Figure 1. The mass–metallicity relation for $z = 2$ star-forming galaxies. Circles represent metallicity measurements where both Hα and [N II] are detected above a 3σ significance level and downward arrows are quoted as [N II]1σ detection limits. The average error in determining the mass of galaxies using ZFOURGE photometry and FAST of ± 0.076 is shown in the bottom left. The dotted horizontal line solar abundance (Asplund et al. 2009). The sample is divided into low ($<10\ M_{\odot}\ \mathrm{yr}^{-1}$) and high ($>10\ M_{\odot}\ \mathrm{yr}^{-1}$) SFR bins. The colored lines are bootstrap fits, with 1σ limits, to the mass–metallicity data for low (orange) and high (blue) star-forming galaxies. The slopes of the fitted data are $m_{\mathrm{SFR}<10} = 0.07 \pm 0.05$ and $m_{\mathrm{SFR}>10} = 0.42 \pm 0.03$ for the low star-forming (SFR $< 10\ M_{\odot}\ \mathrm{yr}^{-1}$) and high star-forming (SFR $> 10\ M_{\odot}\ \mathrm{yr}^{-1}$) galaxies, respectively. (Right) The solid points are stacked spectra within the indicated mass bins and note that these are consistent with the fitted data.
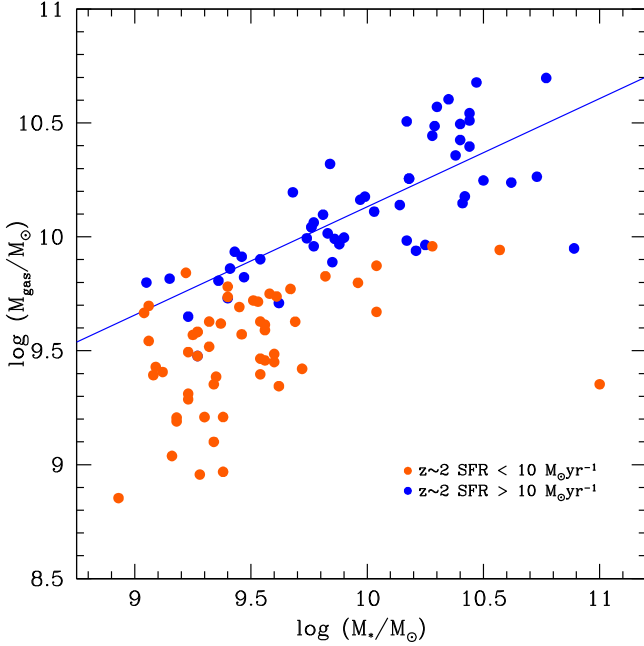

Figure 2. The total gas mass derived using the inverse Kennicutt–Schmidt Law with the adopted the formalism from Papovich et al. (2015). The data are bifurcated at a SFR of $10\ M_{\odot}\ \mathrm{yr}^{-1}$. A line is fit to the high SFR galaxies, which we use to define a gas mass main sequence whereby low SFR galaxies are gas-deficient relative to this main sequence [$M_{\mathrm{gas}} = 10.0 + 0.48(M_* - 10.0)$].

significant amounts of near-to or pristine gas, then this would result in a lower gas-phase metallicity (as seen in Figure 1). If, however, the accretion is low or subsiding, for a fixed mass, the galaxy would have a higher gas-phase metallicity.

In Figure 2, we fit the high star-forming total gas mass as a function of stellar mass as the baseline/main sequence of the total gas expected for an actively accreting galaxy [$M_{\mathrm{gas}} = 10.0 + 0.48(M_* - 10.0)$]. We assume that the low star-forming galaxies are gas-deficient by a known amount, defined by its offset from the fit to the high star-forming main sequence.

We then ask, of the gas that could be added to make deficient galaxies (orange) become a main sequence object (blue), what would its metallicity have to be such that it would reside on the mass–metallicity fitted relation defined by the highly star-forming galaxies (as shown in Figure 1). More simply, the accretion gas mass is computed from the vertical offset of gas-deficient galaxies (orange) from the main sequence fit in Figure 2. The metallicity of the accreted gas is determined from the vertical offset of the low star-forming galaxies (orange) from the best fit of the high star-forming galaxies in Figure 1. Our results are insensitive to the exact slope of our fit. Under these basic assumptions, we can determine the mass and metallicity of gas being accreted in actively accreting galaxies at $z = 2$. We assume an oxygen solar abundance of 8.69 (Asplund et al. 2009) and Z is defined as the ratio of the mass of oxygen in the gas-phase and the hydrogen gas mass. We compute the accretion gas mass and metallicity as follows:

$$\Delta Z \Delta M = Z_f (M_o + \Delta M) - Z_o M_o, \qquad (1)$$

where Z_o is the original metallicity of the metal-rich low star-forming galaxies (orange points in Figure 1), and Z_f is the metallicity main sequence defined by the fit to the high star-forming galaxies shown in Figure 1. M_o is the original gas mass of the gas-deficient low star-forming galaxies (orange points in Figure 2) and ΔM is accreted gas added to M_o such that it
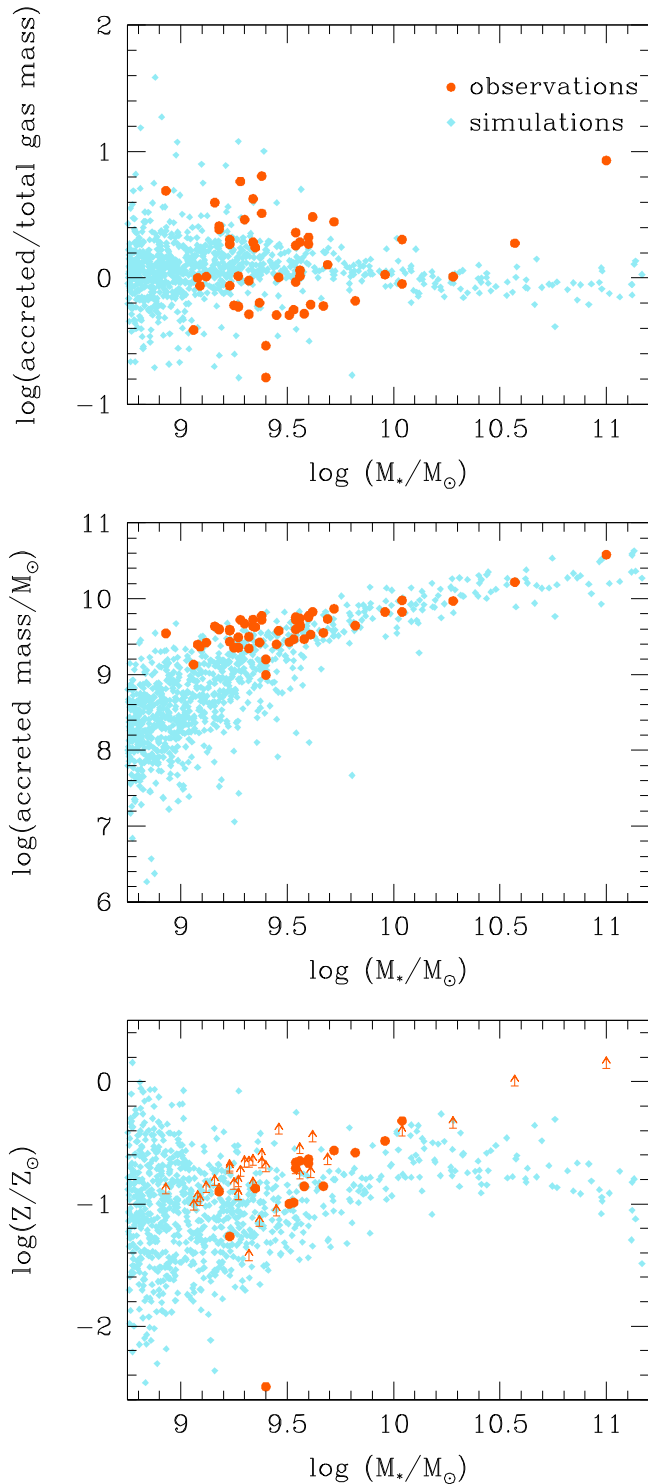
Figure 3. (Top) The computed gas fraction of expected cold-mode accreted gas mass over the total current gas mass for star-forming galaxies as a function of stellar mass from observations (orange). The computed cold-mode accreted gas fraction from the OWLS simulations over the redshift interval of $z = 2$–2.5 (blue). (Middle) The computed total cold-mode accreted gas mass as a function of stellar mass from observations (orange) and simulations (blue). (Bottom) The metallicity of the cold-mode accreted gas mass (shown above) from observations (orange) and from the OWLS simulations over the redshift interval of $z = 2$–2.5 (blue).

contains a total gas mass consistent with the defined gas main sequence in Figure 2. Finally, ΔZ is the metallicity of the gas added (ΔM) required to place the low star-forming galaxies

onto the mass–metallicity relation defined by the high star-forming galaxies as shown in Figure 1.

In Figure 3 (top) we show the fraction of gas required to be added/accreted to the gas-deficient low star-forming galaxies to have a total gas mass that is equivalent to those defined by the high star-forming galaxy main sequence main sequence ($\Delta M/M_o$). The majority of the objects need to acquire/accrete about the same as their existing gas mass and some objects as much as eight times more. The amount of gas required is independent of galaxy stellar mass; however, there is more scatter at low stellar masses. This is expected since accretion events are likely to have the largest effect on a galaxy's total mass when it is low, which is shown in the middle panel of Figure 3. Here, accreted gas mass increases with stellar mass.

Figure 3 (bottom) shows the metallicity required for all of the low star-forming galaxies to fall on the high star-forming galaxy mass–metallicity sequence (see Figure 2, blue fit). There is a trend with galaxy stellar mass, whereby less massive galaxies must accrete lower metallicity gas than higher stellar mass galaxies. The accreted gas has a metallicity range spanning from around -1.5 dex to -0.25 dex from low to high stellar mass, respectively.

3.3. Cosmological Simulations

We compare our observational results to cosmological, hydrodynamical simulations from the OWLS project (Schaye et al. 2010), which uses a modified version of GADGET-3 (Springel 2005). We make use of the "reference" model with cosmological parameters $\Omega_m = 0.238$, $\Omega_b = 0.0418$, $h = 0.73$, $\sigma_8 = 0.74$, $n = 0.951$.

The simulation consists of a $(25 \text{ comoving Mpc } h^{-1})^3$ periodic volume with 512^2 dark matter and 512^2 baryonic particles with initial masses of 8.7×10^6 and $1.9 \times 10^6 \, M_\odot$, respectively. Star formation takes place in gas with density $n_H \geq 0.1 \text{ cm}^{-3}$ and is modeled according to the recipe of Schaye & Dalla Vecchia (2008). Stellar feedback from Type II supernovae is implemented kinetically, following Dalla Vecchia & Schaye (2008), with an initial wind velocity of 600 km s^{-1} and mass loading of 2, which means that a newly formed star particle kicks twice its own mass in neighboring gas particles, on average. The abundances of 11 elements released by massive and intermediate mass stars are followed as described in Wiersma et al. (2009). At $z = 2$, there are 665 massive galaxies with stellar mass above $10^{8.9} \, M_\odot$. We have repeated our analysis for a simulation with eight times lower mass resolution and found our results to be unchanged.

Galaxy stellar mass is measured within a 20 kpc radius centered on the galaxy, including only gravitationally bound particles (using SUBFIND; Dolag et al. 2009). The ISM mass is measured within the same radius, but with the additional requirement that the gas is star-forming ($n_H \geq 0.1 \text{ cm}^{-3}$).

We calculated the accreted gas mass from $z = 2.5$ to $z = 2$, which corresponds to a time interval of 0.70 Gyr, because we found this redshift interval to match the normalization of the observationally derived accreted gas masses. To exclude hot-mode accretion we only consider gas that has never reached a temperature above $10^{5.5}$ K before $z = 2.5$ (van de Voort et al. 2011). The accreted gas mass includes the gas that was in the ISM of the galaxy of interest at $z = 2$ and the gas that was ejected from the ISM between $z = 2.5$ and $z = 2$, but was not in the ISM of any galaxy at $z = 2.5$ (thus excluding mergers). The accreted gas mass includes the gas particles in

the ISM of the galaxy of interest at $z = 2$ and the star particles formed after $z = 2.5$ and the gas particles that were ejected from the ISM between $z = 2.5$ and $z = 2$, which were not in the ISM of any galaxy at $z = 2.5$ (thus excluding mergers). In order to exclude winds from satellites, we only include ejected gas that is closer to the galaxy of interest than any other galaxy.

Figure 3 (top) shows the ratio of the accreted gas mass from $z = 2.5$–2 and the ISM mass at $z = 2$ (blue) along with the data (orange). Over a period of 0.70 Gyr, the galaxy accretes gas masses $\sim$1–2 times greater than its total gas mass, with some scatter to higher and lower values for the lower stellar mass galaxies, which is consistent with our observations. The total gas mass that is accreted is shown in Figure 3 (middle). The data exhibit a similar distribution compared to the simulations, which is dependent on stellar mass. We note that in the simulations, gases originating from hot-mode accretion have total masses that are 1–1.5 dex lower than gas masses originating from cold accretion and are inconsistent with our estimated gas masses from our observations.

The bottom panel of Figure 3 shows the metallicity distribution of accreted gas from $z = 2.5$–2 (blue) along with the observations (orange). The mean metallicity is calculated from the particle metallicities at $z = 2.5$, before the gas accretes onto the galaxy. The gas metallicity is dependent on galaxy stellar mass increasing from low mass to $10^{10}\,M_\odot$, which is likely a direct effect of more massive galaxies enriching their surroundings more quickly compared to less massive galaxies. The trend further decreases at higher masses, which is likely a numerical effect, due to the fact that the $600\ \mathrm{km\ s^{-1}}$ stellar winds are unable to drive significant galactic outflows. This reduces the ratio of recycled gas accretion to accretion from the IGM and thus reduces the mean metallicity. With more efficient feedback at high stellar masses, we expect the trend of increasing metallicity to continue. The simulations and observations are consistent and exhibit similar trends, showing that gas accretion could be responsible for the scatter in the mass–metallicity relation.

4. DISCUSSION

We have identified a fundamental mass–metallicity relation at $z \sim 2$ (4.4σ), whereby galaxies with low SFRs ($<10\,M_\odot\ \mathrm{yr^{-1}}$) exhibit higher metallicities than high star-forming ($<10\,M_\odot\ \mathrm{yr^{-1}}$).

We have examined whether the activity of cold accretion could drive this scatter in the fundamental mass–metallicity relation. Given the simplicity of our assumptions, it is interesting to see that the metallicities and accreted masses required to reduce the scatter in the mass–metallicity relation at $z \sim 2$ are consistent with and show similar trends as in our simulations. Therefore, it is tempting to suggest that gas accretion is solely responsible for the existence of the fundamental mass–metallicity relation. Our conclusions are consistent with previous works at low redshift that attribute the observed scatter in the mass–metallicity relation seen at very low stellar masses to accretion and/or mergers (Bothwell et al. 2013; Forbes et al. 2014). These results demonstrate the direct relationship between cosmological accretion and the fundamental properties of galaxies.

We note that at a fixed metallicity, a higher ionization parameter produces lower [N ii]/Hα ratios and thus lower N2-metallicities (e.g., Kewley & Dopita 2002). The existence of shock will elevate [N ii]/Hα ratios (e.g., Rich et al. 2011; Yuan

et al. 2012). However, we do not think ionization parameters/shocks are the main driver for the scatter of the MZ relation because it is difficult to explain the bifurcation in SFR since the ionization parameter is usually positively correlated with specific SFR. We will study the effect of the ionization parameter and/or shocks in future work.

Our interpretation that accretion drives the fundamental mass–metallicity relation may not be unexpected given that $z \sim 2$ is near the peak epoch of star formation, where outflows are ubiquitous (e.g., Steidel et al. 2010) and cold accretion likely occurs (e.g., Bouché et al. 2013), delivering a significant amount of metal-poor gas to galaxies. These objects are ideal targets for ALMA to determine whether high star-forming galaxies indeed have significantly higher gas fractions and vice versa.

Facility: Keck I (MOSFIRE).

REFERENCES

Asplund, M., Grevesse, N., Sauval, A. J., & Scott, P. 2009, ARA&A, 47, 481
Bothwell, M. S., Maiolino, R., Kennicutt, R., et al. 2013, MNRAS, 433, 1425
Bouché, N., Murphy, M. T., Kacprzak, G. G., et al. 2013, Sci, 341, 50
Bruzual, G., & Charlot, S. 2003, MNRAS, 344, 1000
Calzetti, D., Armus, L., Bohlin, R. C., et al. 2000, ApJ, 533, 682
Cardelli, J. A., Clayton, G. C., & Mathis, J. S. 1989, ApJ, 345, 245
Chabrier, G. 2003, PASP, 115, 763
Cowley, M. J., Spitler, L. R., Tran, K.-V. H., et al. 2016, MNRAS, 457, 629
Crighton, N. H. M., Hennawi, J. F., & Prochaska, J. X. 2013, ApJL, 776, L18
Dalla Vecchia, C., & Schaye, J. 2008, MNRAS, 387, 1431
Dekel, A., Birnboim, Y., Engel, G., et al. 2009, Natur, 457, 451
Dolag, K., Borgani, S., Murante, G., & Springel, V. 2009, MNRAS, 399, 497
Erb, D. K., Shapley, A. E., Pettini, M., et al. 2006, ApJ, 644, 813
Faucher-Giguère, C.-A., Kereš, D., & Ma, C.-P. 2011, MNRAS, 417, 2982
Forbes, J. C., Krumholz, M. R., Burkert, A., & Dekel, A. 2014, MNRAS, 443, 168
Grogin, N. A., Kocevski, D. D., Faber, S. M., et al. 2011, ApJS, 197, 35
Hao, C.-N., Kennicutt, R. C., Johnson, B. D., et al. 2011, ApJ, 741, 124
Kacprzak, G. G., Churchill, C. W., Ceverino, D., et al. 2010, ApJ, 711, 533
Kacprzak, G. G., Churchill, C. W., Steidel, C. C., Spitler, L. R., & Holtzman, J. A. 2012, MNRAS, 427, 3029
Kacprzak, G. G., Yuan, T., Nanayakkara, T., et al. 2015, ApJL, 802, L26
Kereš, D., Katz, N., Weinberg, D. H., & Davé, R. 2005, MNRAS, 363, 2
Kewley, L. J., & Dopita, M. A. 2002, ApJS, 142, 35
Kewley, L. J., Yuan, T., Nanayakkara, T., et al. 2016, ApJ, 819, 100
Koekemoer, A. M., Faber, S. M., Ferguson, H. C., et al. 2011, ApJS, 197, 36
Kriek, M., van Dokkum, P. G., Labbé, I., et al. 2009, ApJ, 700, 221

Nanayakkara, T., Glazebrook, K., Kacprzak, G. G., et al. 2016, ApJS, in press (arXiv:1607.00013)

Maier, C., Ziegler, B. L., Lilly, S. J., et al. 2015, A&A, 577, A14

Mannucci, F., Cresci, G., Maiolino, R., Marconi, A., & Gnerucci, A. 2010, MNRAS, 408, 2115

Papovich, C., Labbé, I., Quadri, R., et al. 2015, ApJ, 803, 26

Pettini, M., & Pagel, B. E. J. 2004, MNRAS, 348, L59

Rich, J. A., Kewley, L. J., & Dopita, M. A. 2011, ApJ, 734, 87

Sánchez Almeida, J., Elmegreen, B. G., Muñoz-Tuñón, C., et al. 2015, ApJL, 810, L15

Sanders, R. L., Shapley, A. E., Kriek, M., et al. 2015, ApJ, 799, 138

Schaye, J., & Dalla Vecchia, C. 2008, MNRAS, 383, 1210

Schaye, J., Dalla Vecchia, C., Booth, C. M., et al. 2010, MNRAS, 402, 1536

Springel, V. 2005, MNRAS, 364, 1105

Steidel, C. C., Erb, D. K., Shapley, A. E., et al. 2010, ApJ, 717, 289

Steidel, C. C., Kollmeier, J. A., Shapely, A. E., et al. 2002, ApJ, 570, 526

Steidel, C. C., Rudie, G. C., Strom, A. L., et al. 2014, ApJ, 795, 165

Straatman, C. M. S., Spitler, L. R., Quadri, R. F., et al. 2016, ApJ, in press

Tran, K.-V. H., Nanayakkara, T., Yuan, T., et al. 2015, ApJ, 811, 28

Tremonti, C. A., Heckman, T. M., Kauffmann, G., et al. 2004, ApJ, 613, 898

Troncoso, P., Maiolino, R., Sommariva, V., et al. 2014, A&A, 563, A58

van de Voort, F., & Schaye, J. 2012, MNRAS, 423, 2991

van de Voort, F., Schaye, J., Booth, C. M., Haas, M. R., & Dalla Vecchia, C. 2011, MNRAS, 414, 2458

van der Wel, A., Bell, E. F., Häussler, B., et al. 2012, ApJS, 203, 24

Wiersma, R. P. C., Schaye, J., Theuns, T., Dalla Vecchia, C., & Tornatore, L. 2009, MNRAS, 399, 574

Wolynetz, M. S. 1979, J. R. Stat. Soc., 28, 195

Yuan, T.-T., Kewley, L. J., Swinbank, A. M., & Richard, J. 2012, ApJ, 759, 66

Yuan, T., Nanayakkara, T., Kacprzak, G. G., et al. 2014, ApJL, 795, L20

Zahid, H. J., Dima, G. I., Kudritzki, R.-P., et al. 2014, ApJ, 791, 130